Seasonal Variability of Phytoplankton Vertical Distribution in a Contrasted South Pacific Ocean From BioGeoChemical-Argo Profiling Floats

T. Hermilly, E. Martinez, J. Uitz, M. Cornec, N. Kolodziejczyk, C. Schmechtig

Geophysical Research Letters

RESEARCH LETTER
10.1029/2024GL114262

Seasonal Variability of Phytoplankton Vertical Distribution in a Contrasted South Pacific Ocean From BioGeoChemical-Argo Profiling Floats

T. Hermilly[1], E. Martinez[1], J. Uitz[2], M. Cornec[3,4], N. Kolodziejczyk[1], and C. Schmechtig[5]

[1]University of Western Brittany, CNRS, Ifremer, IRD, Laboratoire d'Océanographie Physique et Spatiale (LOPS), IUEM, Plouzané, France, [2]Laboratoire d'Océanographie de Villefranche (LOV), UMR 7093, CNRS, Sorbonne Université, Villefranche-sur-mer, France, [3]School of Oceanography University of Washington, Seattle, WA, USA, [4]NOAA/OAR Pacific Marine Environmental Laboratory, Seattle, WA, USA, [5]OSU Ecce Terra, UAR 3455, CNRS, Sorbonne Université, Paris Cedex, France

Abstract The seasonal variability of phytoplankton vertical distribution is investigated in the South Pacific where observations are scarce and scattered. We used 13 BioGeoChemical-Argo floats deployed across diverse oceanic environments. The seasonal latitudinal displacement of the Tasman front induces transitions from mesotrophic to oligotrophic conditions. This shift results in Chlorophyll-a concentration vertical distribution changing from bloom types to Subsurface Chlorophyll Maxima (SCM) types, with intermediate hybrid types between these extremes. Such hybrid profiles frequently occur in the equatorial Pacific, highlighting a large-scale pattern rather than local island mass effect. In oligotrophic regions, seasonal variations of light availability and stratification dynamics below the mixed layer likely relate SCM to an increase in carbon biomass or photoacclimation. A biomass increase is frequently observed, contrary to previous studies, suggesting that subsurface phytoplankton biomass may have been largely underestimated. This calls for further observations of the water column in these remote undersampled open ocean areas.

Plain Language Summary This study investigates the seasonal variability of the vertical distribution of Chlorophyll-a concentration (Chl, a proxy of phytoplankton biomass) in the South Pacific. We analyze observations from 13 autonomous BioGeoChemical-Argo profiling floats deployed in contrasted biogeochemical areas. The considered nutrient-limited (oligotrophic) regions encompass the central South Pacific Gyre, the Fiji-Tonga area and the Coral Sea. Regions where nutrient availability is higher (mesotrophic) are also considered, notably the equatorial zone and the Tasman Sea. Oligotrophic regions host persistent Subsurface Chl Maxima (SCM) either driven by phytoplankton carbon biomass increases or physiological adaptation to low light conditions. Indeed, seasonal mixing and water column destabilization likely enhance nutrients in the SCM layer, supporting phytoplankton growth. The Tasman front, separating nutrient-poor northern waters from nutrient-rich southern waters, shifts seasonally in latitude. Therefore, Chl profiles may show oligotrophic conditions (low surface Chl and SCM) or mesotrophic conditions (higher surface Chl and homogeneous distribution), depending on the front position. In the equatorial region, the frequent occurrence of hybrid Chl profiles—featuring relatively high surface Chl and SCM—appears to result from the regional ocean dynamics rather than the influence of nearby islands. These findings highlight the need for further studies in remote, nutrient-limited regions of the open ocean.

Key Points:

- We report contrasted seasonal variations of phytoplankton vertical distribution in the undersampled South Pacific from 13 BGC-Argo floats
- In oligotrophic gyres, subsurface carbon biomass influenced by stratification below the mixed layer may have been largely underestimated
- Equatorial waters show Chlorophyll-a profiles associating moderately high surface values with a subsurface maximum

Supporting Information:

Supporting Information may be found in the online version of this article.

Correspondence to:

T. Hermilly,
thomas.hermilly@ird.fr

Citation:

Hermilly, T., Martinez, E., Uitz, J., Cornec, M., Kolodziejczyk, N., & Schmechtig, C. (2025). Seasonal variability of phytoplankton vertical distribution in a contrasted South Pacific Ocean from BioGeoChemical-Argo profiling floats. *Geophysical Research Letters*, *52*, e2024GL114262. https://doi.org/10.1029/2024GL114262

Received 13 DEC 2024
Accepted 17 JUL 2025

Author Contributions:

Conceptualization: T. Hermilly, E. Martinez, J. Uitz
Formal analysis: T. Hermilly, E. Martinez, J. Uitz, M. Cornec, N. Kolodziejczyk
Funding acquisition: E. Martinez, J. Uitz
Investigation: T. Hermilly, N. Kolodziejczyk
Methodology: T. Hermilly, E. Martinez, J. Uitz, M. Cornec, N. Kolodziejczyk, C. Schmechtig
Project administration: E. Martinez

1. Introduction

Phytoplankton, at the basis of the marine food web, play a key role for the oceanic upper trophic levels and carbon export to the deep ocean. Hence, it is essential to characterize the spatio-temporal variability of their biomass. Phytoplankton growth relies on the availability of light and nutrients, the latter being made available in the sunlit layer through oceanic and atmospheric processes. Specifically, changes in the water column stratification due to vertical mixing can induce the uplift of nutrients from the deep ocean to the euphotic zone, hence allowing phytoplankton to grow (e.g., Eppley et al., 1979; Gačić et al., 2002; Peeters et al., 2013). Conversely, intense stratification, such as in the oligotrophic gyres, prevents nutrient uplift (e.g., Lewis et al., 1986; Moore et al., 2013; Strom & Fredrickson, 2008). Under certain conditions, phytoplankton cells may be found in a deeper layer of the water column, at a depth where light and nutrients availability is balanced (Cullen, 2015; Morel et al., 2010). Such subsurface maxima are well-documented through observations of Chlorophyll-a concentration

Software: T. Hermilly, M. Cornec, C. Schmechtig
Supervision: E. Martinez, J. Uitz
Writing – original draft: T. Hermilly, E. Martinez, J. Uitz, M. Cornec

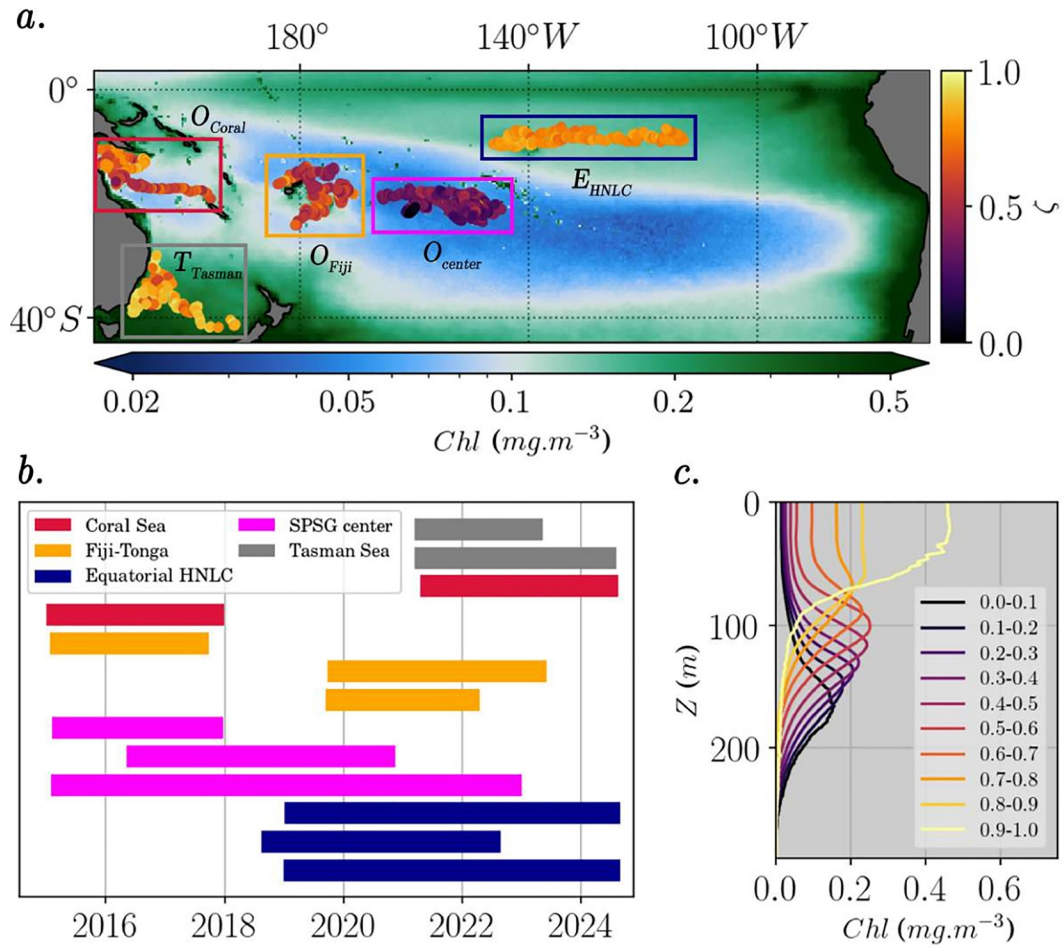

Figure 1. (a) Trajectories of the 13 BGC-Argo floats. Each dot represents the location of a float profile with its ζ value in color as presented in (c). ζ is an indicator of the shape of the Chl vertical profile (vertical colorbar). Boxes delineate the five distinct regions of float drift, namely the Tasman Sea (T_{Tasman}), the Coral Sea (O_{Coral}), the Fiji-Tonga region (O_{Fiji}), the center of the South Pacific Subtropical Gyre (O_{center}) and the equatorial HNLC area (E_{HNLC}). The color in background is the surface Chl from the OC-CCI satellite product averaged over 2015–2023 (horizontal colorbar). (b) Timeline of Chl measurements for each BGC-Argo float, with colors corresponding to float drift regions as in (a). (c) Range of ζ values corresponding to the Chl vertical profiles. The associated Chl values are indicated as the *X*-axis.

(Chl), a proxy for phytoplankton biomass. They are referred to as Deep Chlorophyll Maxima (DCM) or Subsurface Chlorophyll Maxima (SCM; e.g., Cullen, 2015; Shulenberger & Reid, 1981). Albeit widely used, Chl is nevertheless an ambiguous proxy, as the Chl-to-carbon biomass ratio depends on phytoplankton composition and physiology and, in particular, changes with depth due to the physiological response of phytoplankton cells to light-limited conditions, a process called photoacclimation (Geider, 1987). Hence, SCM distributions do not always reflect a concomitant increase in Chl and carbon biomass at depth (i.e., Subsurface Biomass Maxima, SBM), but instead an increase of Chl associated with photoacclimation (i.e., Subsurface Acclimation Maxima, SAM; e.g., Barbieux et al., 2019; Cornec et al., 2021). The latter being likely associated with reduced biological production in oligotrophic environments (e.g., Barbieux et al., 2022), the distinction between these two processes is crucial to study the biological carbon pump and ecosystem dynamics (e.g., Westberry et al., 2008). However, environmental processes associated with the formation of SAM or SBM remain poorly understood, even at the seasonal scale.

The vast South Pacific Ocean (SPO) encompasses a variety of biogeochemical environments. It hosts the largest oligotrophic area of the global ocean, with strong stratification inducing relatively low mean surface Chl (<0.1 mg m^{-3}; Claustre & Maritorena, 2003; Morel et al., 2010; Figure 1a). This area itself is contrasted, ranging

from moderate oligotrophy in the western tropical SPO (≃0.1 mg m^{-3}) to extreme oligotrophy (≃0.01 mg m^{-3}) in the vicinity of Easter Island (Claustre et al., 2008). Observations from few oceanic cruises in the South Pacific Subtropical Gyre (SPSG) have revealed spatial differences in the subsurface layer considering the depth and intensity of the SCM, but also the composition of phytoplankton communities (Bonnet et al., 2023; Claustre et al., 2008; Moutin et al., 2017; Ras et al., 2008). In addition, only two studies focused on the investigation of the seasonal variability of Chl vertical distributions in this region, using only 1 year of observations from a BioGeoChemical-Argo (BGC-Argo) profiling float each (Mignot et al., 2014; Sauzède et al., 2020). However, how this seasonal variability is modulated along a longitudinal gradient in the oligotrophic SPSG, as well as the relative importance of SAM versus SBM and the underlying physical and biogeochemical processes have never been investigated.

The oligotrophic SPSG is surrounded by mesotrophic environments along the equatorial band as well as at temperate and high latitudes. North of the SPSG, the equatorial divergence induces High Nutrient Low Chlorophyll (HNLC) conditions (Murray et al., 1992) which may be disturbed by the presence of islands such as the Marquesas Islands (Cassianides et al., 2020; Martinez & Maamaatuaiahutapu, 2004; Raapoto et al., 2019). Observations based on one oceanographic cruise and one year deployment of a BGC-Argo float allowed the investigation of the vertical structure of Chl within this archipelago in 2011–2012 (Martinez et al., 2020). The Chl vertical profiles appeared to alternate between well-mixed distributions (i.e., homogeneous distribution of Chl in the mixed layer) and a combination of well-mixed and SCM patterns along a north-south gradient. However the authors could not specify whether the Chl vertical distribution combining these two types of profiles was induced by particular biogeochemical properties of the HNLC area or by the presence of the islands (Island Mass Effect, IME; Doty & Oguri, 1956), nor by some regional and/or seasonal forcings.

At temperate latitudes at the SPO western boundary, the Tasman Sea straddles the Tasman Front, which represents an eastern extension of the East Australian Current. This current separates from the east coast of Australia at a seasonal scale (Kerry & Roughan, 2020) and meanders towards the northern tip of New Zealand (Oke et al., 2019). North of the front, the stratified, oligotrophic Coral Sea waters are relatively unproductive, while the vertically well-mixed waters south of the front exhibit strong biological activity (Baird et al., 2008). Studies on phytoplankton based on *in situ* observations focused on the North-East Tasman Sea (Ellwood et al., 2013) or on the western region close to the Australian East coast (e.g., Baird et al., 2008; Suthers et al., 2011). Within the Tasman Sea, to our knowledge, only two satellite based studies have investigated the Chl variability at a seasonal scale but observations were limited to the surface (Chiswell et al., 2013; Tilburg et al., 2002). Here again, the seasonal variability of the vertical dynamics of Chl at the scale of the Tasman front remains unclear.

Over the last decade, the BGC-Argo program has drastically increased the number of *in situ* measurements of key physical and biogeochemical variables, in particular in remote, poorly sampled regions like the SPO. Recent studies based on this program investigated the seasonal variability of Chl vertical distributions at the global scale (Bock et al., 2022; Cornec et al., 2021), the North Atlantic Ocean (Lacour et al., 2019) or the Mediterranean Sea (Barbieux et al., 2019). In contrast, a specific focus on the SPO has never been performed, so that the seasonal variability of the Chl vertical distribution in this basin remains largely unknown, as well as the physical-biogeochemical processes at stake. Here, we use observations from 13 BGC-Argo profiling floats that drifted from 2015 to 2023 in the contrasted SPO provinces presented above (Figures 1a and 1b), namely the temperate-latitude Tasman Sea (T_{Tasman}), the equatorial HNLC area (E_{HNLC}), and three oligotrophic regions following a zonal gradient from the Coral Sea (O_{Coral}) and the Fiji-Tonga region (O_{Fiji}) to the center of the SPSG (O_{center}). The aim of the present study is to characterize the seasonal variability of the Chl vertical distribution in these regions and to investigate the underlying physical-biogeochemical mechanisms. A focus is placed on the SAM and SBM seasonality along the east-west gradient of the SPSG.

2. Data and Methods

2.1. Processing of the BGC-Argo Measurements

We use observations from 13 BGC-Argo profiling floats (Figures 1a and 1b), deployed in the Tasman and Coral Seas, the vicinity of the Fiji and Tonga archipelagos, the center of the SPO, and the Equatorial HNLC area (see the World Meteorological Organization numbers, Table S1 in the Supporting Information S1). All the floats are equipped with a Sea-Bird Scientific SBE41 CTD sensor measuring temperature (T), salinity (S), and pressure (P), a Sea-Bird ECO Puck that measures Chlorophyll-*a* fluorescence (excitation/emission wavelengths of 470/

695 nm) and the particulate backscattering coefficient at 700 nm (b_{bp}), a Sea-Bird OCR-504 multispectral radiometer that measures the Photosynthetic Available Radiation (PAR) as well as the downwelling irradiance at 380 nm ($E_d(380)$), 412 nm ($E_d(412)$), and 490 nm ($E_d(490)$). Apart from two floats in O_{center}, all the floats are also equipped with Anderaa optodes measuring dissolved oxygen concentration.

The Chlorophyll-*a* fluorescence and b_{bp} coefficient are derived from the raw optical signal of the ECO sensor following the standard BGC-Argo protocol (Carval et al., 2018; Dall'Olmo et al., 2023; Schmechtig et al., 2015, 2023). To account and correct for the strong regional variability in the fluorescence-to-Chl ratio (Petit et al., 2022; Roesler et al., 2017), we assess a conversion factor for each vertical profiles using the $E_d(490)$ measurements as described by Xing et al. (2011). Each float is attributed a constant correction factor, corresponding to the median values obtained over its lifetime. The resulting factors are consistent with Petit et al. (2022) and Roesler et al. (2017) in the SPSG. Finally, the Chl profiles are smoothed with a 10-m moving average and corrected from Non-Photochemical Quenching (NPQ) following Terrats et al. (2020). Spikes potentially associated with particle aggregates or zooplankton may be observed in b_{bp} profiles (Briggs et al., 2011; Haëntjens et al., 2020). A 10-m moving average is applied to the b_{bp} individual profiles, and values exceeding the 5th and 95th percentiles of the residuals are removed, following Barbieux et al. (2019).

The PAR profiles are corrected from cloud effects which intermittently reduces irradiance values. To do so, an envelope is derived for each log-transformed PAR profile, using strictly decreasing and moving-average filters with a 50-m window. The difference between observations and the envelope is used with a threshold to identify the occurrence of clouds. Finally, following Organelli et al. (2016), a 4th-degree beta-spline curve is fitted to the observations not affected by clouds (see details in Text S1 in Supporting Information S1).

For most of the floats used in this study, the profiling frequency is 5 days. However, some of the floats cycled at a higher frequency (1–3 days) during few months after deployment. In this case, only the profiles acquired every 5 days are considered for consistency.

2.2. Classification of the Chl Vertical Profiles

As in Mignot et al. (2011), two mathematical functions illustrating two main types of Chl vertical profiles—Bloom and SCM—are adjusted to the BGC-Argo Chl profiles (see Text S2 in Supporting Information S1). The SCM type is characterized by a pronounced subsurface peak, while the Bloom type shows elevated values in the upper layer and a well mixed distribution below. Then, the quality of each fit is assessed using the squared Pearson correlation coefficient, r^2, and the Chl profiles are assigned with the Bloom or SCM types according to the best statistics. In addition, we include a Hybrid type for the Chl profiles when both functions have satisfying fits (i.e., $r^2 > 0.8$). This type corresponds to profiles featuring significant surface values associated with a notable subsurface maximum. Finally, the Chl profiles for which the fit scores are too low ($r^2 < 0.8$) for both models are classified as Other and discarded (less than 1%). As a result, 12% of the profiles belong to the Bloom type, 75% to the SCM type and 12% to the Hybrid type.

This approach also allows the retrieval of the SCM depth (Z_{SCM}) and width (W_{SCM}) for the Chl profiles of the SCM type, as adjustment parameters of the gaussian model (see Text S3 in Supporting Information S1). The Chl profiles from the SCM type are further classified in two subcategories to determine whether the SCM is related to the occurrence of a carbon biomass maximum concomitant with the Chl maximum (i.e., SBM) or to photo-acclimation of phytoplankton cells to low light conditions at depth (i.e., SAM). Following Cornec et al. (2021), vertical profiles of b_{bp}, which can be used as a proxy for the stock of Particulate Organic Carbon (POC), are considered in addition to the Chl profiles. Correlations between Chl and b_{bp} are calculated along depth over the layer $[Z_{SCM} - W_{SCM}; Z_{SCM} + W_{SCM}]$ for each profile. Significant correlation means that a subsurface local maximum of b_{bp} is detected in the vicinity of Z_{SCM}, thus the SCM is considered as a SBM. Inversely, the SCM is considered as a SAM when there is no significant correlation between Chl and b_{bp}. Hence, this classification yields to four types that are Bloom, Hybrid, SAM and SBM, with the last two corresponding to profiles of the SCM type. The full method is detailed in Text S4 in Supporting Information S1.

2.3. An Indicator of the Shape of Chl Vertical Profiles (ζ)

Here we propose a novel indicator, ζ, that provides a synthetic, quantitative view of the spatio-temporal variability of the Chl vertical distribution at the SPO scale. The method to derive ζ relies on the Principal Component

Analysis of the whole data set of Chl profiles (see Text S5 in Supporting Information S1). Notably, ζ well reproduces the two profile types exhibited in Mignot et al. (2011), that is Bloom and SCM, through a single one-dimensional parameter suitable for a wider range of profile shapes. Indeed, it smoothly connects the sigmoid (reflecting the Bloom type, with higher values of ζ) and gaussian shapes (reflecting the SCM type, with lower values of ζ), passing through the Hybrid type associated with intermediate values of ζ (Figure 1c). Therefore, ζ provides information about SCM characteristics such as Z_{SCM}, W_{SCM}, as well as surface and SCM Chl values.

2.4. Hydrological Variables

BGC-Argo measurements are used to investigate the physical and biogeochemical mechanisms driving the Chl vertical distribution and seasonal variability. As stratification plays a key role in nutrient uplift toward the sunlit layer, here we consider two variables based on potential density (computed using the Gibbs-SeaWater library; McDougall & Barker, 2011). First, the mixed layer depth (MLD) is used to trace the surface-driven mixing. It is defined as the depth at which surface density is exceeded by 0.125 kg m^{-3}, a density criterion usually considered in the study region (Ohno et al., 2004; Sauzède et al., 2020; Suga et al., 2004). Then, the squared Brunt-Vaisala frequency (N^2, or buoyancy frequency) is also estimated, as it is commonly used as an indicator of ocean stratification (Agustí & Duarte, 1999). Its maximum depth (Z_{N2max}) is a proxy for the pycnocline depth (Lü et al., 2020), which is more independent from surface properties than the MLD (Strutton et al., 2023). It is defined as:

$$N^2(z) = -\frac{g}{\rho_0}\,\partial_z\sigma(z)$$

with z the depth, g the gravitational acceleration, ρ_0 the mean density of seawater (taken as 1,025 kg m^{-3}), ∂_z the z-wise derivative operator and σ the potential density referenced to the surface.

In regions such as the subtropics, the presence of a surface salinity maximum leads to destabilizing the salinity vertical profile. During winter, the convective mixing generates a strongly density-compensated layer at the base of the well-mixed layer. This structure can lead to the occurrence of double-diffusive convection (Kolodziejczyk & Gaillard, 2012, 2013; Yeager & Large, 2007). This phenomenon can be illustrated by the Turner angle (Ruddick, 1983):

$$T_u(z) = \tan^{-1}\left(\frac{\alpha\partial_z T(z) + \beta\partial_z S(z)}{\alpha\partial_z T(z) - \beta\partial_z S(z)}\right)$$

with respectively α and β the sea water thermal expansion and haline contraction coefficients. Values of T_u within $\pm 45°$ correspond to depths where the water column is doubly stable. $T_u > 45°$ indicates that the salinity gradient is destabilizing and the temperature gradient is stabilizing. Inversely, $T_u < -45°$ indicates that the temperature gradient is destabilizing and the salinity gradient is stabilizing. The process of double-diffusive convection can occur when $T_u > 71.6°$ (Ruddick, 1983). Probability that $T_u > 71.6°$ is computed considering the mean and standard deviation of T_u, assuming a normal distribution.

Light penetration is quantified through the depth of the 20 µmol quanta m^{-2} s^{-1} isolume (Z_{iso20}) using the PAR data from the BGC-Argo floats, as in Barbieux et al. (2019) and Cornec et al. (2021).

Lastly, the CANYON-B neural network is applied to pressure, temperature, salinity, oxygen (Table S1 in Supporting Information S1 to see oxygen sensor availability), position and date data from the BGC-Argo floats to derive nitrate concentration. To ensure robust predictions, this neural network was trained on both climatological (GLODAPv2; Olsen et al., 2020) and bottle data from various oceanographic cruises within the global ocean (Bittig et al., 2018; Sauzède et al., 2017). The nitracline depth, Z_{nit}, is then calculated as the depth of the 1 µmol L^{-1} isoline (Cermeño et al., 2008; Lavigne et al., 2015; Sauzède et al., 2020).

For all considered variables, monthly climatologies are calculated from the individual profiles.

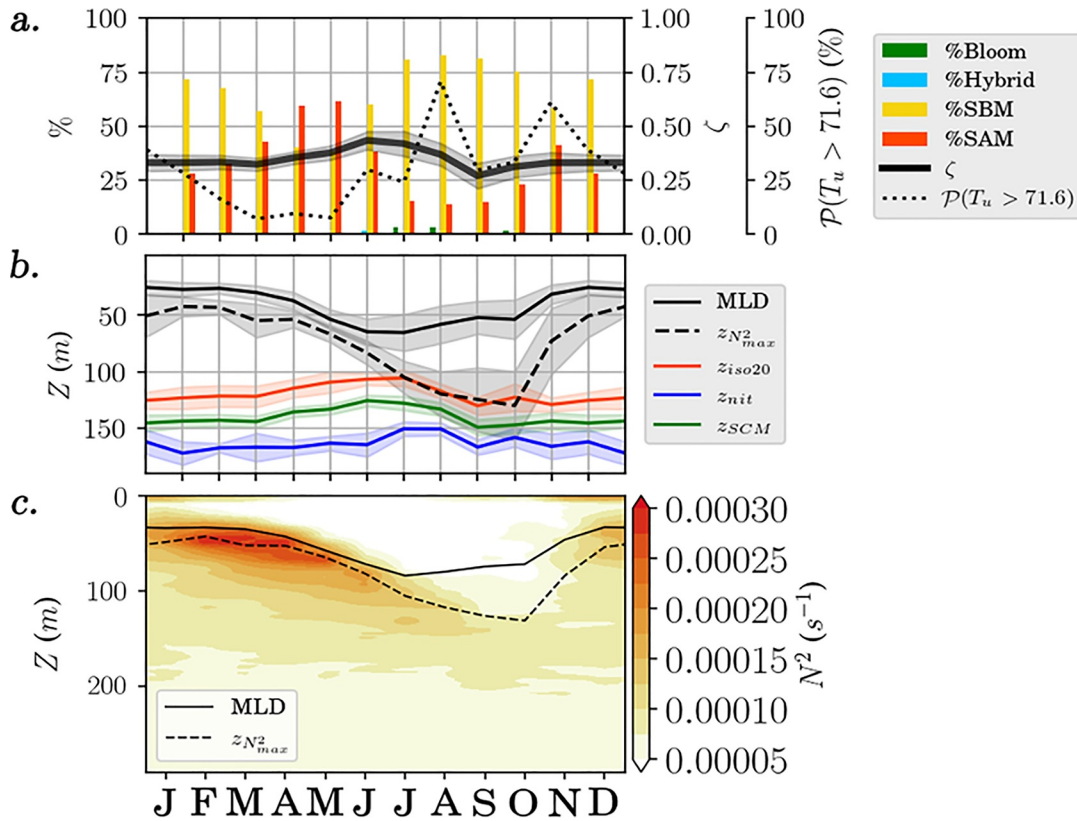

Figure 2. Seasonal climatologies for O_{center} of: (a) the percentage of Chl profile types (Bloom, Hybrid, SBM and SAM; left axis), ζ values (first right axis, solid black line), and probability of T_u being >71.6 (second right axis, dash black line); (b) MLD, Z_{N2max}, Z_{iso20}, Z_{nit} and Z_{SCM} along depth; (c) N^2 along depth. MLD and Z_{N2max} as in (b) are reported.

3. Results and Discussion

At the basin scale, ζ provides a synoptic view about the different types of Chl vertical profiles within the SPO (Figure 1a). The lowest seasonal values of ζ ($\simeq$0.25), in O_{center} (Figure 1a), are associated with the deepest SCM (down to 140 m) and the lowest surface Chl ($\simeq$0.02 mg m^{-3}; Figure 1c). Intermediate values of ζ ($0.5 < \zeta < 0.7$) can be observed in O_{Coral} and O_{Fiji} reflecting shallower Z_{SCM} (~100 m) and higher surface Chl values (0.05 mg m^{-3}) along a zonal gradient toward the western oligotrophic area. E_{HNLC} and T_{Tasman} mesotrophic areas are associated with the Bloom and Hybrid types ($\zeta > 0.85$ and $0.75 < \zeta < 0.85$, respectively). In addition to providing a synoptic view of the SPO spatial variability in the Chl vertical distributions, ζ also allows investigating their seasonal variations.

3.1. The Zonal Gradient of the South Pacific Oligotrophic Gyre

In the O_{center} region, ζ shows weak, yet notable seasonal variations. Minimum ζ values ($\simeq$0.25, Figure 2a) are observed from September to March and are associated with a deep SCM compared to other oligotrophic regions ($Z_{SCM} \simeq 150$ m; Figure 2b). In contrast, maximum ζ values (0.45) are found during the austral winter (July), when the SCM is the shallowest ($Z_{SCM} \sim 125$ m). These results are consistent with a permanent SCM regime reported in several previous studies (e.g., Cornec et al., 2021; Dandonneau et al., 2004; Mignot et al., 2014). Here, it is related to a MLD permanently 100–150 m shallower than Z_{nit} (Figure 2b), illustrating that the seasonal convection cannot reach the nitracline and uplift nutrients toward the upper sunlit layer in this area. Also, seasonal variations of the SCM depth are light-driven as illustrated by a Z_{SCM} closely following Z_{iso20} ($r = 0.93$; Figure 2b; Mignot et al., 2014).

Although Chl vertical profiles of SCM type dominate throughout the year in the O_{center} region, the relative contribution of SAM (induced by photoacclimation) or SBM (associated with an increase in carbon biomass) is

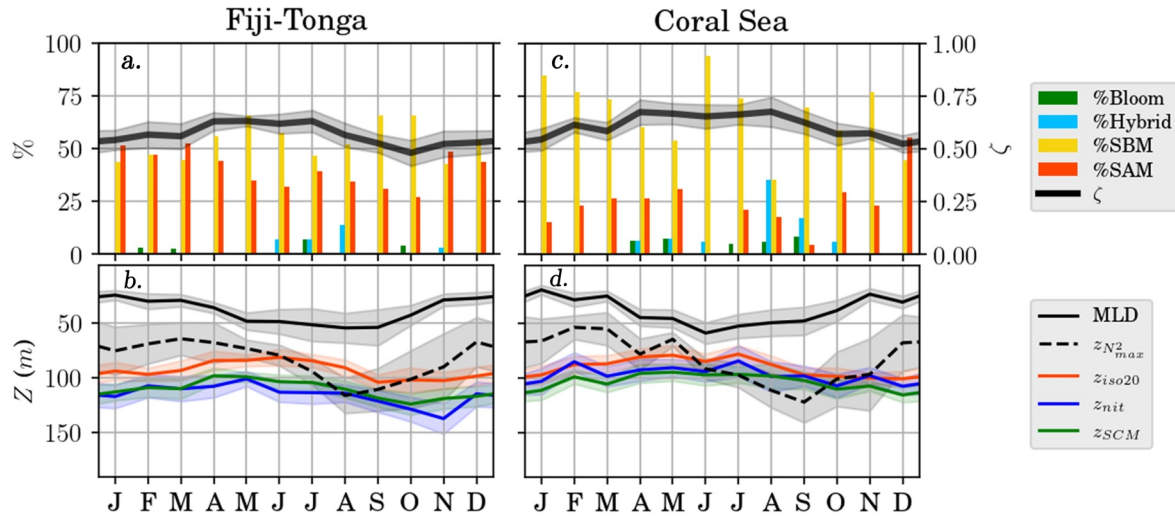

Figure 3. (a, c) Same as Figure 2a without the information about T_u for O_{Fiji} and O_{Coral}, respectively. (b, d) Same as Figure 2b, also for O_{Fiji} and O_{Coral}, respectively.

highly variable on a seasonal scale. SAM profiles dominate and reach their maximum occurrence frequency (60%) in April–May (late autumn/early winter in the southern hemisphere). SBM profiles dominate throughout the rest of the year, with a maximum contribution (80%) in the July–October period (late winter/spring). These observations contrast with previous studies in permanently stratified oligotrophic regions indicating a dominance of SBM only in summer (December–March) likely due to a Z_{SCM} closer to the nitrate pool following the seasonal isolume deepening (Barbieux et al., 2019; Cornec et al., 2021; Mignot et al., 2014).

To understand the dominance of the SBM type in June–October, we investigate the variations of N^2 which provides additional information about stratification and vertical stability of the water column (Figure 2c). Indeed, O_{center} has particular hydrodynamic properties as the South Pacific Tropical Water (SPTW) is characterized by a vertical salinity maximum (35.6–36.5 psu) located at 8°S−25°S, 160°W−110°W, lying in the upper thermocline around the 25 kg m^{-3} isopycnal (Qu et al., 2013; Tsuchiya & Talley, 1996). In winter/spring, stratification weakens (Figure 2c) and the depth of its maximum Z_{N2max} deepens well below the MLD (Figures 2b and 2c). This suggests stronger convection and vertical mixing leading to the formation of density-compensated layers between the base of the mixed layer and the pycnocline (Kolodziejczyk & Gaillard, 2013; Yeager & Large, 2007). Enhanced vertical mixing may erode the nitracline and allow nutrient diffusion at these depths (although mixing may not be strong enough to extend up to the surface). In addition, an enhanced compensated layer is likely to favor double diffusive mixing (of nutrients) as supported by the values of the Turner angle (high percentage of values >71.6). This ensemble of processes could explain the significant occurrence of SBM, which would rely on local vertical supply of nutrients.

Oligotrophic characteristics can also be observed in the O_{Fiji} and O_{Coral} regions. The seasonal variations of ζ follow those of Z_{SCM} (Figures 3a and 3b), and the MLD remains 70–100 m above Z_{nit} (Figures 3c and 3d). However, from O_{Center} to O_{Fiji} and O_{Coral}, both Z_{nit} and Z_{iso20} are uplifted and get closer to each other, inducing a Z_{SCM} 30–40 m shallower in O_{Coral} than O_{center}. In addition, the westward deepening of the tropical-subtropical pycnocline and Z_{N2max} in the SPO (Johnson & McPhaden, 1999) associated with a shallower Z_{nit} could allow nutrient inputs at Z_{SCM} and induce a higher occurrence of SBM than in O_{Center}. Finally, such a nutrient input in the surface layer likely occurs in August and September when the stratification is the weakest and Z_{N2max} deepens below Z_{nit}. This would induce the appearance of Bloom and Hybrid type profiles. The sporadic occurrence of the Hybrid and Bloom types among the other months of the year may rather reflect the supply of nutrients from a relatively shallow Z_{nit} associated with specific phenomena such as the influence of Pacific islands (Messié et al., 2020, 2022), hydrothermal sources supplying iron as reported in O_{Fiji} (Guieu et al., 2018; Tilliette et al., 2022), or eddies and front activity (Heywood et al., 1996; Travis & Qiu, 2020).

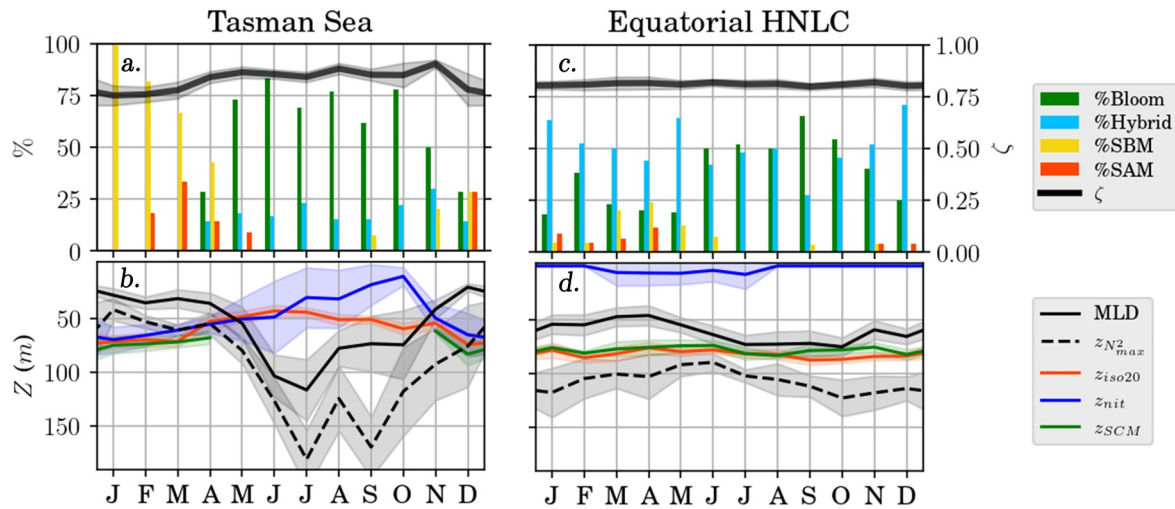

Figure 4. As in Figure 3 but for (a, b) T_{Tasman}, and (c, d) E_{HNLC}.

3.2. The Productive Mid-Latitude Tasman Sea and Equatorial HNLC Area

At temperate latitudes, higher Chl in the Tasman front when compared to the oligotrophic areas is partly related to the mixing of relatively warm, macronutrient-poor but iron-rich oligotrophic water from the subtropics with cooler, macronutrient-rich but iron-poor subantarctic water (Boyd et al., 1999). In this region, ζ reaches high values (0.75–0.9, Figure 4a) compared to the overall low values found in the three oligotrophic regions. From January to April, the predominance of the SCM type profiles reflects a southward shift of the front and a positioning of the floats in an oligotrophic environment with MLDs shallower than Z_{nit} (Figures 4b and S6.1a in Supporting Information S1). The predominance of SBM is explained by Z_{nit} and Z_{iso20} approximately located at the same depth. From March to October, the Tasman front has moved northward and the floats are located in a mesotrophic environment (Figures S6.1b and S6.1c in Supporting Information S1). The predominance of the Bloom type profiles reflects two dynamical processes. First, the occurrence of a bloom coincides with the gradual deepening of the mixed layer from April to July (Figure 4b; Figure S6.2 in Supporting Information S1). Then, the bloom goes on as the MLD shoals while light and nitrate availability increase from August to November (Figure 4b; Figure S6.3 in Supporting Information S1). These blooms and MLD dynamics coincide with the surface Chl seasonal variability reported by Tilburg et al. (2002) from three years of satellite observations in the Tasman Sea over 37°S–42°S. Finally, as the Tasman front moves southward at the end of the year, the successive changes of dominance from Bloom to Hybrid, and then to SCM type profiles (at the beginning of the year) illustrate the transition from a mesotrophic to oligotrophic environment.

The E_{HNLC} area is also related to a productive regime with ζ values about 0.8, reflecting the Hybrid and Bloom type profiles, and very few occurrences of the SCM type (Figure 4c). Unlike in the Tasman Sea, Z_{nit} either reaches or is close to the surface, highlighting the expected no-limiting nitrate conditions (Figure 4d). The Hybrid type profiles dominate all over the year. The consumption of nitrates at the surface could explain Chl values $\simeq$0.2 mg m^{-3}, consistent with satellite observations, while the SCM-like type reflects higher Chl as nitrate concentrations increase with depth. The trajectories of the four BGC-Argo floats, mainly upstream of the Marquesas archipelago, suggest that these types of Chl profiles are related to the regional HNLC environment, rather than to the local Marquesas IME. Finally, the Bloom type profile occurrence increases from July to November following the seasonal deepening of the MLD, and a subsequent stronger input of nutrients toward the mixed layer. Conversely, the SBM type occasionally occurs in March and April when the MLD is the shallowest.

4. Conclusion

This study provides the first seasonal climatology of Chl vertical distribution in the South Pacific Ocean using BGC-Argo profiling floats. By refining previous general classification methods (based on a distinction between Bloom profiles and Subsurface Chlorophyll Maxima profiles, SCM), it also includes distinctions between SCM

profiles driven by photoacclimation (SAM) or biomass increase (SBM), and Hybrid types (intermediate between SCM and Bloom profiles), along with a new index (ζ) for profile shape comparison. The results reveal a permanent deep SCM in the oligotrophic O_{center}, O_{Fiji}, and O_{Coral} regions. A north-westward gradient is observed, with an uplift of the nitracline and SCM depths and a deepening of the pycnocline leading to increased SBM and Hybrid type profiles in the west. In the Tasman Sea, contrasting oligotrophic and mesotrophic environments show seasonal SBM and Bloom type dominance north and south of the Tasman front, respectively. Finally, in the E_{HNLC} the high occurrence of Hybrid type profiles is the imprint of the regional HNLC environment rather than local island mass effects.

Stratification-related metrics (e.g., N^2 and Z_{N2max}) appear to better explain the difference in the seasonal occurrence of SAM and SBM profiles in oligotrophic areas, compared to the dynamics of the MLD alone. This result suggests that stratification and potential double-diffusion events would play a key role in vertical nutrient inputs toward the upper layers in oligotrophic environments.

These findings also highlight the need to distinguish between SBM and SAM processes, as SBM-dominated profiles, potentially associated with increased biological production, are more frequent in the oligotrophic SPO than previously reported. Thus, it is crucial to keep on expanding *in situ* biogeochemical observations, in particular in the poorly sampled SPO, in order to understand long-term changes in primary production and carbon export in response to ongoing and future climate warming.

Conflict of Interest

The authors declare no conflicts of interest relevant to this study.

Data Availability Statement

The BGC Argo data can be freely downloaded on https://doi.org/10.17882/42182 (Argo, 2025). The OC-CCI satellite Chl product with a 4 km daily resolution over 2015–2023 was downloaded from https://data.marine.copernicus.eu/product/OCEANCOLOUR_GLO_BGC_L3_MY_009_107. All analyses have been performed using python 3.11.3. The code behind the CANYON-B estimation of nitrate concentration from temperature, salinity and oxygen concentration is available openly at https://github.com/HCBScienceProducts/CANYON-B.

Acknowledgments
This work represents a contribution to the following research projects: THOT, MOANA MATY, OUTPACE, and TONGA, which benefited from BGC-Argo floats from the LEFE GMMC program (CNRS-INSU) as a contribution to the French segment of the BGC-Argo program. This work is also a contribution to Argo-2030 which received the support of the French government within the framework of the Program "Investissements d'Avenir" integrated in France 2030 and managed by the Agence Nationale de la Recherche (ANR) under the reference ANR-21-ESRE-0019. The BGC-Argo data were collected and made freely available by the International Argo Program and the national programs that contribute to it (http://www.argo.ucsd.edu, http://argo.jcommops.org/). This Argo Program is part of the Global Ocean Observing System. The deployments of all the floats (except in the Tasman Sea) have been supported by the French oceanographic fleet. This work was supported by CNRS INSU LEFE CYBER French national program within the framework of the Moana Maty project, as well as the government of French Polynesia for the financial support of the Moana O Te Ati Enana project (convention °07498°). We would like to thank the Government of French Polynesia and the French State for providing funding support to the THOT project (Contrat de projets Etat-Pays, convention n°8690/MSR/REC, and arrêté de subvention n° HC/2860/DIE/BPT). The PhD grant of T. Hermilly was co-funded by a doctoral research grant from the French Brittany region (Allocations de recherche doctorale, ARED) and the French National Research Institute for sustainable Development (IRD). M. Cornec. was supported by the National Science Foundation (award: OCE, 2023274/2147809 to A. J. Fassbender), National Oceanic and Atmospheric Administration (NOAA) Global Ocean Monitoring and Observing program, and NOAA Pacific Marine Environmental Laboratory.

References

Agustí, S., & Duarte, C. M. (1999). Phytoplankton chlorophyll a distribution and water column stability in the central Atlantic Ocean. *Oceanologica Acta*, *22*(2), 193–203. https://doi.org/10.1016/S0399-1784(99)80045-0

Argo. (2025). Argo float data and metadata from Global Data Assembly Centre (Argo GDAC) [Dataset]. *SEANOE*. https://doi.org/10.17882/42182

Baird, M. E., Timko, P. G., Middleton, J. H., Mullaney, T. J., Cox, D. R., & Suthers, I. M. (2008). Biological properties across the Tasman Front off southeast Australia. *Deep Sea Research Part I: Oceanographic Research Papers*, *55*(11), 1438–1455. https://doi.org/10.1016/j.dsr.2008.06.011

Barbieux, M., Uitz, J., Gentili, B., Pasqueron de Fommervault, O., Mignot, A., Poteau, A., et al. (2019). Bio-optical characterization of subsurface chlorophyll maxima in the Mediterranean Sea from a Biogeochemical-Argo float database. *Biogeosciences*, *16*(6), 1321–1342. https://doi.org/10.5194/bg-16-1321-2019

Barbieux, M., Uitz, J., Mignot, A., Roesler, C., Claustre, H., Gentili, B., et al. (2022). Biological production in two contrasted regions of the Mediterranean Sea during the oligotrophic period: An estimate based on the diel cycle of optical properties measured by BioGeoChemical-Argo profiling floats. *Biogeosciences*, *19*(4), 1165–1194. https://doi.org/10.5194/bg-19-1165-2022

Bittig, H. C., Steinhoff, T., Claustre, H., Fiedler, B., Williams, N. L., Sauzède, R., et al. (2018). An alternative to static climatologies: Robust estimation of open ocean CO2 variables and nutrient concentrations from T, S, and O2 data using Bayesian neural networks. *Frontiers in Marine Science*, *5*, 328. https://doi.org/10.3389/fmars.2018.00328

Bock, N., Cornec, M., Claustre, H., & Duhamel, S. (2022). Biogeographical classification of the Global Ocean from BGC-Argo floats. *Global Biogeochemical Cycles*, *36*(6), e2021GB007233. https://doi.org/10.1029/2021GB007233

Bonnet, S., Guieu, C., Taillandier, V., Boulart, C., Bouruet-Aubertot, P., Gazeau, F., et al. (2023). Natural iron fertilization by shallow hydrothermal sources fuels diazotroph blooms in the ocean. *Science*, *380*(6647), 812–817. https://doi.org/10.1126/science.abq4654

Boyd, P., LaRoche, J., Gall, M., Frew, R., & McKay, R. M. L. (1999). Role of iron, light, and silicate in controlling algal biomass in subantarctic waters SE of New Zealand. *Journal of Geophysical Research*, *104*(C6), 13395–13408. https://doi.org/10.1029/1999JC900009

Briggs, N., Perry, M. J., Cetinić, I., Lee, C., D'Asaro, E., Gray, A. M., & Rehm, E. (2011). High-resolution observations of aggregate flux during a sub-polar North Atlantic spring bloom. *Deep Sea Research Part I: Oceanographic Research Papers*, *58*(10), 1031–1039. https://doi.org/10.1016/j.dsr.2011.07.007

Carval, T., Coatanoan, C., Schmechtig, C., Racape, V., Rannou, J. P., & Dobler, D. (2018). *Processing Bio-Argo particle backscattering at the DAC level (version 1.4)*. Ifremer. https://doi.org/10.13155/39459

Cassianides, A., Martinez, E., Maes, C., Carton, X., & Gorgues, T. (2020). Monitoring the influence of the Mesoscale Ocean dynamics on phytoplanktonic plumes around the marquesas Islands using multi-satellite missions. *Remote Sensing*, *12*(16), 2520. https://doi.org/10.3390/rs12162520

Cermeño, P., Dutkiewicz, S., Harris, R. P., Follows, M., Schofield, O., & Falkowski, P. G. (2008). The role of nutricline depth in regulating the ocean carbon cycle. *Proceedings of the National Academy of Sciences*, *105*(51), 20344–20349. https://doi.org/10.1073/pnas.0811302106

Chiswell, S. M., Bradford-Grieve, J., Hadfield, M. G., & Kennan, S. C. (2013). Climatology of surface chlorophyll a, autumn-winter and spring blooms in the southwest Pacific Ocean. *Journal of Geophysical Research: Oceans*, *118*(2), 1003–1018. https://doi.org/10.1002/jgrc.20088

Claustre, H., & Maritorena, S. (2003). The many shades of ocean blue. *Science*, *302*(5650), 1514–1515. https://doi.org/10.1126/science.1092704

Claustre, H., Sciandra, A., & Vaulot, D. (2008). Introduction to the special section bio-optical and biogeochemical conditions in the South East Pacific in late 2004: The BIOSOPE program. *Biogeosciences*, *5*(3), 679–691. https://doi.org/10.5194/bg-5-679-2008

Cornec, M., Claustre, H., Mignot, A., Guidi, L., Lacour, L., Poteau, A., et al. (2021). Deep chlorophyll maxima in the global ocean: Occurrences, drivers and characteristics. *Global Biogeochemical Cycles*, *35*(4), e2020GB006759. https://doi.org/10.1029/2020GB006759

Cullen, J. J. (2015). Subsurface chlorophyll maximum layers: Enduring enigma or mystery solved? In *Annual review of marine science* (Vol. 7(7), pp. 207–239). Annual Reviews. https://doi.org/10.1146/annurev-marine-010213-135111

Dall'Olmo, G., Bhaskar Tvs, U., Bittig, H., Boss, E., Brewster, J., Claustre, H., et al. (2023). *BGC Argo quality control manual for particles backscattering (version 1.0)*. Ifremer. https://doi.org/10.13155/60262

Dandonneau, Y., Deschamps, P.-Y., Nicolas, J.-M., Loisel, H., Blanchot, J., Montel, Y., et al. (2004). Seasonal and interannual variability of ocean color and composition of phytoplankton communities in the North Atlantic, equatorial Pacific and South Pacific. *Deep Sea Research Part II: Topical Studies in Oceanography*, *51*(1), 303–318. https://doi.org/10.1016/j.dsr2.2003.07.018

Doty, M. S., & Oguri, M. (1956). The Island mass effect. *ICES Journal of Marine Science*, *22*(1), 33–37. https://doi.org/10.1093/icesjms/22.1.33

Ellwood, M. J., Law, C. S., Hall, J., Woodward, E. M. S., Strzepek, R., Kuparinen, J., et al. (2013). Relationships between nutrient stocks and inventories and phytoplankton physiological status along an oligotrophic meridional transect in the Tasman Sea. *Deep Sea Research Part I: Oceanographic Research Papers*, *72*, 102–120. https://doi.org/10.1016/j.dsr.2012.11.001

Eppley, R. W., Renger, E. H., & Harrison, W. G. (1979). Nitrate and phytoplankton production in southern California coastal waters 1. *Limnology & Oceanography*, *24*(3), 483–494. https://doi.org/10.4319/lo.1979.24.3.0483

Gačić, M., Civitarese, G., Miserocchi, S., Cardin, V., Crise, A., & Mauri, E. (2002). The open-ocean convection in the Southern Adriatic: A controlling mechanism of the spring phytoplankton bloom. *Continental Shelf Research*, *22*(14), 1897–1908. https://doi.org/10.1016/S0278-4343(02)00050-X

Geider, R. J. (1987). Light and temperature dependence of the carbon to chlorophyll a ratio in microalgae and cyanobacteria: Implications for physiology and growth of phytoplankton. *New Phytologist*, *106*(1), 1–34. https://doi.org/10.1111/j.1469-8137.1987.tb04788.x

Guieu, C., Bonnet, S., Petrenko, A., Menkes, C., Chavagnac, V., Desboeufs, K., et al. (2018). Iron from a submarine source impacts the productive layer of the Western Tropical South Pacific (WTSP). *Scientific Reports*, *8*(1), 9075. https://doi.org/10.1038/s41598-018-27407-z

Haëntjens, N., Della Penna, A., Briggs, N., Karp-Boss, L., Gaube, P., Claustre, H., & Boss, E. (2020). Detecting mesopelagic organisms using biogeochemical-Argo floats. *Geophysical Research Letters*, *47*(6), e2019GL086088. https://doi.org/10.1029/2019GL086088

Heywood, K. J., Stevens, D. P., & Bigg, G. R. (1996). Eddy formation behind the tropical island of Aldabra. *Deep Sea Research Part I: Oceanographic Research Papers*, *43*(4), 555–578. https://doi.org/10.1016/0967-0637(96)00097-0

Johnson, G. C., & McPhaden, M. J. (1999). Interior pycnocline flow from the subtropical to the equatorial Pacific Ocean. *Journal of Physical Oceanography*, *29*(12), 3073–3089. https://doi.org/10.1175/1520-0485(1999)029<3073:IPFFTS>2.0.CO;2

Kerry, C., & Roughan, M. (2020). Downstream evolution of the East Australian Current System: Mean flow, seasonal, and intra-annual variability. *Journal of Geophysical Research: Oceans*, *125*(5), e2019JC015227. https://doi.org/10.1029/2019JC015227

Kolodziejczyk, N., & Gaillard, F. (2012). Observation of spiciness interannual variability in the Pacific pycnocline. *Journal of Geophysical Research*, *117*(C12), 2012JC008365. https://doi.org/10.1029/2012JC008365

Kolodziejczyk, N., & Gaillard, F. (2013). Variability of the heat and salt budget in the subtropical Southeastern Pacific mixed layer between 2004 and 2010: Spice injection mechanism. *Journal of Physical Oceanography*, *43*(9), 1880–1898. https://doi.org/10.1175/JPO-D-13-04.1

Lacour, L., Briggs, N., Claustre, H., Ardyna, M., & Dall'Olmo, G. (2019). The intraseasonal dynamics of the mixed layer pump in the subpolar North Atlantic Ocean: A biogeochemical-Argo float approach. *Global Biogeochemical Cycles*, *33*(3), 266–281. https://doi.org/10.1029/2018GB005997

Lavigne, H., D'Ortenzio, F., Ribera D'Alcalà, M., Claustre, H., Sauzède, R., & Gacic, M. (2015). On the vertical distribution of the chlorophyll a concentration in the Mediterranean Sea: A basin-scale and seasonal approach. *Biogeosciences*, *12*(16), 5021–5039. https://doi.org/10.5194/bg-12-5021-2015

Lewis, M. R., Hebert, D., Harrison, W. G., Platt, T., & Oakey, N. S. (1986). Vertical nitrate fluxes in the oligotrophic Ocean. *Science*, *234*(4778), 870–873. https://doi.org/10.1126/science.234.4778.870

Lü, H., Zhao, X., Sun, J., Zha, G., Xi, J., & Cai, S. (2020). A case study of a phytoplankton bloom triggered by a tropical cyclone and cyclonic eddies. *PLoS One*, *15*(4), 1–18. https://doi.org/10.1371/journal.pone.0230394

Martinez, E., & Maamaatuaiahutapu, K. (2004). Island mass effect in the Marquesas Islands: Time variation. *Geophysical Research Letters*, *31*(18). https://doi.org/10.1029/2004GL020682

Martinez, E., Rodier, M., Pagano, M., & Sauzède, R. (2020). Plankton spatial variability within the Marquesas archipelago, South Pacific. *Journal of Marine Systems*, *212*, 103432. https://doi.org/10.1016/j.jmarsys.2020.103432

McDougall, T. J., & Barker, P. M. (2011). Getting started with TEOS-10 and the Gibbs Seawater (GSW) oceanographic toolbox. *Scor/iapso WG*, *127*(532), 1–28.

Messié, M., Petrenko, A., Doglioli, A. M., Aldebert, C., Martinez, E., Koenig, G., et al. (2020). The delayed Island mass effect: How Islands can remotely trigger blooms in the oligotrophic Ocean. *Geophysical Research Letters*, *47*(2), e2019GL085282. https://doi.org/10.1029/2019GL085282

Messié, M., Petrenko, A., Doglioli, A. M., Martinez, E., & Alvain, S. (2022). Basin-scale biogeochemical and ecological impacts of islands in the tropical Pacific Ocean. *Nature Geoscience*, *15*(6), 469–474. https://doi.org/10.1038/s41561-022-00957-8

Mignot, A., Claustre, H., D'Ortenzio, F., Xing, X., Poteau, A., & Ras, J. (2011). From the shape of the vertical profile of in vivo fluorescence to Chlorophyll-a concentration. *Biogeosciences*, *8*(8), 2391–2406. https://doi.org/10.5194/bg-8-2391-2011

Mignot, A., Claustre, H., Uitz, J., Poteau, A., D'Ortenzio, F., & Xing, X. (2014). Understanding the seasonal dynamics of phytoplankton biomass and the deep chlorophyll maximum in oligotrophic environments: A Bio-Argo float investigation. *Global Biogeochemical Cycles*, *28*(8), 856–876. https://doi.org/10.1002/2013GB004781

Moore, C. M., Mills, M. M., Arrigo, K. R., Berman-Frank, I., Bopp, L., Boyd, P. W., et al. (2013). Processes and patterns of oceanic nutrient limitation. *Nature Geoscience*, *6*(9), 701–710. https://doi.org/10.1038/ngeo1765

Morel, A., Claustre, H., & Gentili, B. (2010). The most oligotrophic subtropical zones of the global ocean: Similarities and differences in terms of chlorophyll and yellow substance. *Biogeosciences*, *7*(10), 3139–3151. https://doi.org/10.5194/bg-7-3139-2010

Moutin, T., Doglioli, A. M., de Verneil, A., & Bonnet, S. (2017). Preface: The Oligotrophy to the UlTra-oligotrophy PACific Experiment (OUTPACE cruise, 18 February to 3 April 2015). *Biogeosciences*, *14*(13), 3207–3220. https://doi.org/10.5194/bg-14-3207-2017

Murray, J., Leinen, M., Feely, R., Toggweiler, R., & Wanninkhof, R. (1992). EqPac: A process Study in the central equatorial Pacific. *Oceanography*, *5*(3), 134–142. https://doi.org/10.5670/oceanog.1992.01

Ohno, Y., Kobayashi, T., Iwasaka, N., & Suga, T. (2004). The mixed layer depth in the North Pacific as detected by the Argo floats. *Geophysical Research Letters*, *31*(11), 2004GL019576. https://doi.org/10.1029/2004GL019576

Oke, P. R., Pilo, G. S., Ridgway, K., Kiss, A., & Rykova, T. (2019). A search for the Tasman Front. *Journal of Marine Systems*, *199*, 103217. https://doi.org/10.1016/j.jmarsys.2019.103217

Olsen, A., Lange, N., Key, R. M., Tanhua, T., Bittig, H. C., Kozyr, A., et al. (2020). An updated version of the global interior ocean biogeochemical data product, GLODAPv2.2020. *Earth System Science Data*, *12*(4), 3653–3678. https://doi.org/10.5194/essd-12-3653-2020

Organelli, E., Claustre, H., Bricaud, A., Schmechtig, C., Poteau, A., Xing, X., et al. (2016). A novel near-real-time quality-control procedure for radiometric profiles measured by bio-Argo floats: Protocols and performances. *Journal of Atmospheric and Oceanic Technology*, *33*(5), 937–951. https://doi.org/10.1175/JTECH-D-15-0193.1

Peeters, F., Kerimoglu, O., & Straile, D. (2013). Implications of seasonal mixing for phytoplankton production and bloom development. *Theoretical Ecology*, *6*(2), 115–129. https://doi.org/10.1007/s12080-012-0164-2

Petit, F., Uitz, J., Schmechtig, C., Dimier, C., Ras, J., Poteau, A., et al. (2022). Influence of the phytoplankton community composition on the in situ fluorescence signal: Implication for an improved estimation of the chlorophyll-a concentration from BioGeoChemical-Argo profiling floats. *Frontiers in Marine Science*, *9*, 959131. https://doi.org/10.3389/fmars.2022.959131

Qu, T., Gao, S., & Fine, R. A. (2013). Subduction of South Pacific tropical water and its equatorward pathways as shown by a simulated passive tracer. *Journal of Physical Oceanography*, *43*(8), 1551–1565. https://doi.org/10.1175/JPO-D-12-0180.1

Raapoto, H., Martinez, E., Petrenko, A., Doglioli, A., Gorgues, T., Sauzède, R., et al. (2019). Role of iron in the Marquesas Island mass effect. *Journal of Geophysical Research: Oceans*, *124*(11), 7781–7796. https://doi.org/10.1029/2019JC015275

Ras, J., Claustre, H., & Uitz, J. (2008). Spatial variability of phytoplankton pigment distributions in the Subtropical South Pacific Ocean: Comparison between in situ and predicted data. *Biogeosciences*, *5*(2), 353–369. https://doi.org/10.5194/bg-5-353-2008

Roesler, C., Uitz, J., Claustre, H., Boss, E., Xing, X., Organelli, E., et al. (2017). Recommendations for obtaining unbiased chlorophyll estimates from in situ chlorophyll fluorometers: A global analysis of WET Labs ECO sensors. *Limnology and Oceanography: Methods*, *15*(6), 572–585. https://doi.org/10.1002/lom3.10185

Ruddick, B. (1983). A practical indicator of the stability of the water column to double-diffusive activity. *Deep-Sea Research, Part A: Oceanographic Research Papers*, *30*(10), 1105–1107. https://doi.org/10.1016/0198-0149(83)90063-8

Sauzède, R., Bittig, H. C., Claustre, H., Pasqueron De Fommervault, O., Gattuso, J.-P., Legendre, L., & Johnson, K. S. (2017). Estimates of water-column nutrient concentrations and Carbonate System parameters in the global ocean: A novel approach based on neural networks. *Frontiers in Marine Science*, *4*, 128. https://doi.org/10.3389/fmars.2017.00128

Sauzède, R., Martinez, E., Maes, C., de Fommervault, O. P., Poteau, A., Mignot, A., et al. (2020). Enhancement of phytoplankton biomass leeward of Tahiti as observed by Biogeochemical-Argo floats. *Journal of Marine Systems*, *204*, 103284. https://doi.org/10.1016/j.jmarsys.2019.103284

Schmechtig, C., Claustre, H., Poteau, A., D'Ortenzio, F., Schallenberg, C., Trull, T., & Xing, X. (2023). *BGC-Argo quality control manual for the Chlorophyll-A concentration (version 3.0)*. Ifremer. https://doi.org/10.13155/35385

Schmechtig, C., Poteau, A., Claustre, H., D'Ortenzio, F., & Boss, E. (2015). *Processing BGC-Argo chlorophyll-A concentration at the DAC level (version 1.0)*. Ifremer. https://doi.org/10.13155/39468

Shulenberger, E., & Reid, J. L. (1981). The Pacific shallow oxygen maximum, deep chlorophyll maximum, and primary productivity, reconsidered. *Deep-Sea Research, Part A: Oceanographic Research Papers*, *28*(9), 901–919. https://doi.org/10.1016/0198-0149(81)90009-1

Strom, S. L., & Fredrickson, K. A. (2008). Intense stratification leads to phytoplankton nutrient limitation and reduced microzooplankton grazing in the southeastern Bering Sea. *Deep Sea Research Part II: Topical Studies in Oceanography*, *55*(16–17), 1761–1774. https://doi.org/10.1016/j.dsr2.2008.04.008

Strutton, P. G., Trull, T. W., Phillips, H. E., Duran, E. R., & Pump, S. (2023). Biogeochemical Argo floats reveal the evolution of subsurface chlorophyll and particulate organic carbon in Southeast Indian Ocean eddies. *Journal of Geophysical Research: Oceans*, *128*(4), e2022JC018984. https://doi.org/10.1029/2022JC018984

Suga, T., Motoki, K., Aoki, Y., & Macdonald, A. M. (2004). The north Pacific climatology of winter mixed layer and mode waters. *Journal of Physical Oceanography*, *34*(1), 3–22. https://doi.org/10.1175/1520-0485(2004)034<0003:TNPCOW>2.0.CO;2

Suthers, I. M., Young, J. W., Baird, M. E., Roughan, M., Everett, J. D., Brassington, G. B., et al. (2011). The strengthening east Australian Current, its eddies and biological effects—An introduction and overview. *Deep Sea Research Part II: Topical Studies in Oceanography*, *58*(5), 538–546. https://doi.org/10.1016/j.dsr2.2010.09.029

Terrats, L., Claustre, H., Cornec, M., Mangin, A., & Neukermans, G. (2020). Detection of Coccolithophore blooms with BioGeoChemical-Argo floats. *Geophysical Research Letters*, *47*(23), e2020GL090559. https://doi.org/10.1029/2020GL090559

Tilburg, C. E., Subrahmanyam, B., & O'Brien, J. J. (2002). Ocean color variability in the Tasman Sea. *Geophysical Research Letters*, *29*(10), 125-1–125-4. https://doi.org/10.1029/2001GL014071

Tilliette, C., Taillandier, V., Bouruet-Aubertot, P., Grima, N., Maes, C., Montanes, M., et al. (2022). Dissolved Iron patterns impacted by shallow hydrothermal sources along a transect through the Tonga-Kermadec Arc. *Global Biogeochemical Cycles*, *36*(7), e2022GB007363. https://doi.org/10.1029/2022GB007363

Travis, S., & Qiu, B. (2020). Seasonal reversal of the near-surface chlorophyll response to the presence of mesoscale eddies in the South Pacific subtropical countercurrent. *Journal of Geophysical Research: Oceans*, *125*(3), e2019JC015752. https://doi.org/10.1029/2019JC015752

Tsuchiya, M., & Talley, L. D. (1996). Water-property distributions along an eastern Pacific hydrographic section at 135W. *Journal of Marine Research*, *54*(3), 541–564. https://doi.org/10.1357/0022240963213583

Westberry, T., Behrenfeld, M. J., Siegel, D. A., & Boss, E. (2008). Carbon-based primary productivity modeling with vertically resolved photoacclimation. *Global Biogeochemical Cycles*, *22*(2). https://doi.org/10.1029/2007GB003078

Xing, X., Morel, A., Claustre, H., Antoine, D., D'Ortenzio, F., Poteau, A., & Mignot, A. (2011). Combined processing and mutual interpretation of radiometry and fluorimetry from autonomous profiling Bio-Argo floats: Chlorophyll a retrieval. *Journal of Geophysical Research*, *116*(C6), C06020. https://doi.org/10.1029/2010JC006899

Yeager, S. G., & Large, W. G. (2007). Observational evidence of winter spice injection. *Journal of Physical Oceanography*, *37*(12), 2895–2919. https://doi.org/10.1175/2007JPO3629.1